MEDIAN RESIDENCE AND DISPERSION TIMES FOR FLUIDIZATION OF CRUSHED OIL SHALE

David E. Christiansen and Richard G. Mallon
Lawrence Livermore National Laboratory
P.O. Box 808, L-207
Livermore, CA 94550

ABSTRACT

Median residence times and dispersions for crushed oil shale flowing downward through a fluidized bed were measured as a function of particle size, nominal residence time, and fluidizing gas velocity. For fluidized beds containing narrow particle-size distribution, it was found that median residence time and dispersion increase with nominal residence time, decrease with increasing gas velocity, and show mixed results with change in particle size.

The results for fluidized beds of broad particle-size distribution were different. Increasing the nominal residence time increased the median residence time but had no regular effect upon dispersion. The gas velocity was observed to have a strong effect upon dispersion but little effect upon median residence time. When particle-size effects in this broad particle-size bed were investigated, it was found that the finer particles had a longer median residence time and were more widely dispersed than the coarser particles.

INTRODUCTION

Fluidized beds exhibit processing features which would be useful in the retorting of oil shale. Retorting of oil shale is heat transfer intensive, and therefore one seeks processing techniques which are known for high heat transfer rates; among the best of these is the fluidized bed. Retorting yields are enhanced by rapid separation of the pyrolysis products from the shale; fluidized bed processes provide the required rapid separation. Fluidized beds are also able to handle solids in much the same fashion as liquids are handled in liquid processing equipment--a distinct advantage when large quantities of solids are to be processed. Lastly, the uniform conditions usually experienced in a fluidized bed contribute to the ease of process control. Thus fluidized beds exhibit many worthwhile characteristics that could be useful to the processing of oil shale.

There remain many unanswered questions regarding the use of fluidized beds for processing oil shale in spite of their potential for this use and their long history in petroleum refining. First, how do such beds behave with broad particle-size distributions. In the history of fluidized beds nearly all uses have involved narrow particle-size distributions; hence little is known about what happens when solids of broad particle-size distribution are treated in a fluidized bed. Although earlier work[1] at this laboratory has verified a theoretical method for estimation of a mean particle size for incipient fluidization calculations, there is little information concerning the relative motion of particle-size fractions within a bed; that is, size-dependent dispersion and residence times. Second, given the answer to the first question, what modifications might be made to improve processing conditions such as making residence times more uniform. And third, how might the knowledge of solids behavior in a fluidized bed be incorporated into a mathematical process model so as to obtain an accurate representation of actual performance in, say, a different and perhaps more complex processing system.

THEORY

Current theory does not adequately describe the very complex flow of solids in a fluidized bed. Experimental observations have revealed several mechanisms for solids flow in a bed. As bubbles move upwards starting at the bottom of the bed, they pull threads of solid with them in such a fashion that particles from the bottom of the bed will mark the bubble path throughout the height of the bed. This flow mechanism, in effect, creates a discontinuity in terms of particle age or character as a function of lateral position. Meanwhile there is a compensating downward flow of solids. The

bubbles are also thought to contribute some lateral mixing as they pass. Thus, as a first approximation, it appears that there are three important flow mechanisms to be considered in a gas fluidized or bubbling bed: (1) a macroscopic flow of solids from the solids inlet to the solids outlet, (2) an upward flow of solids drawn by the bubbles, and (3) a local mixing or dispersion also driven by the rising bubbles.

Unfortunately in spite of good efforts, there has been no rigorous treatment of this problem. An approach to such a treatment[2] is to assume that the solids flow has two components: (1) a uniform average solids velocity superposed on which is (2) a dispersive flow described much like gaseous diffusion. This assumption has met with some success in the description of gas flow in packed beds. However, because of the mechanism of the solids flow as described above, this model is not expected to describe the motion of solids in a gas fluidized bed.

EXPERIMENT

In these experiments crushed raw oil shale was fluidized in a bed with air at atmospheric pressure and temperature. This bed was equipped with bins and feeders so that a downward flow of shale could be maintained throughout its effective height. The shale was obtained from the Anvil Points, Colorado, mine and had a grade of 100 L/Mg. Radioactive shale samples were introduced at the top of the bed and their downward passage through the bed was traced by means of radiation detectors.

The experimental effort involved concepts from several quite separate technologies. The fluidized bed and its ancillary equipment (feed hopper, star valves, distributor plate, gas control and measurement equipment, and filters) are common to chemical engineering. The tracer material, neutron activated shale, and detectors take their principles from nuclear physics. The signal conditioning and recording equipment finds place in electrical engineering. Data processing comes from computer technology. Each of these areas will be described in this section.

The fluidized bed was 14 cm (inside diameter) by 175 cm (high) with an active (solids filled) depth of 75 cm. This bed was air-fluidized and was equipped to have solids flowing through it. The solids, crushed oil shale, were fed from a hopper through a star valve into the top of the active portion of the bed (see Figure 1). As shown, the bed had a height of 100 cm above the active portion for solids disentrainment. A tube, fitted with a funnel and valve, was inserted into the top of the bed for introduction of tagged solids. This tube extended downward to about 15 cm above the active portion of the bed. A slender cone was positioned below the end of the tube, 7 cm above the active bed, to spread the tagged solids over the full cross section. The bed was equipped with a rotameter, pressure gage, and temperature indicator to measure the flow of fluidizing air. Differential pressure indicators were used to measure the bed and distributor pressure drops.

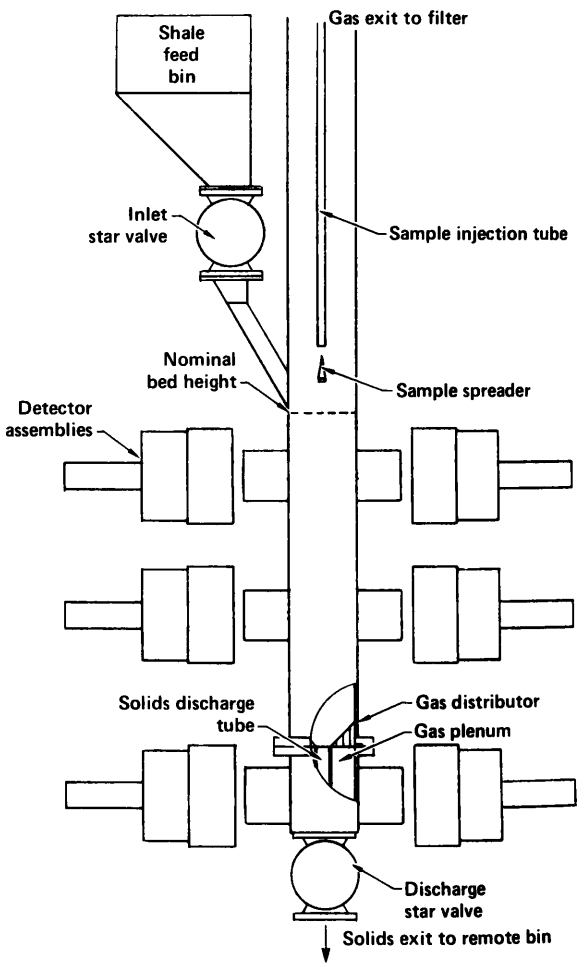

FIGURE 1 - Experimental fluidized bed assembly.

The gas distributor used in this bed was a conical perforated plate with perforations designed to give a pressure drop of 25 to 40% of the bed pressure drop. To cover the range of operating conditions found in these experiments three plates with different perforation diameters were used. Because a flat distributor plate tends to produce regions of stagnant solids, the gas distributors used in these experiments were made conical to eliminate such regions. As the figure also shows, the solids leave the bed through a 3.2-cm-diameter hole in the center of the distributor, descend through a tube, and exit through a star valve. From the star valve the solids were picked up by an industrial vacuum cleaner and transferred to a bin about 10 m away. The solids were moved away from the bed to eliminate the stray count that otherwise would interfere with the bottom detectors during an experiment.

For these experiments the shale was tagged by exposing it to neutrons from the Rotating Target Neutron Source II at the Lawrence Livermore National Laboratory. This facility produces 14 MeV neutrons.[3] The neutrons cause the formation of radioactive ^{28}Al from the aluminum and silicon in the shale by means of two nuclear reactions: (1) conversion of ^{27}Al, as in

$$^{27}Al(n, \gamma)^{28}Al ,$$

and (2) conversion of ^{28}Si, as in

$$^{28}Si(n,p)^{28}Al .$$

The thermal neutrons required for the first reaction were obtained by placing about 15 cm of polyethylene between the source and the sample. This thermalized a portion of the neutron flux for the first reaction, yet left the balance of the flux as fast neutrons for the second reaction. In these experiments, an extremely small fraction of the aluminum and silicon was converted. About one-half of the ^{28}Al was produced by each reaction.

Now, ^{28}Al decays by the reaction

$$^{28}Al \xrightarrow{\beta} {}^{28}Si .$$

This reaction also results in the emission of a 1.78 MeV gamma ray which is of sufficient energy to exit through the walls of the bed and be detected some distance away with very little attenuation. The 138.6-s half-life of the ^{28}Al makes it ideal for this type of experiment. This half-life is sufficiently long for experiments lasting for a few hundred seconds, yet sufficiently short to give strong radiation from the tagged particles and, also very important, after 1000 to 2000 s the tagged particles in the solids are sufficiently inactive that the solids can be used again in the next experiment. Also, because of this short half-life, the shale is essentially at saturation activity with respect to the ^{28}Al with only a 600-s neutron exposure. Because the neutron exposure is so short there is but little activation of other isotopes which are longer lived. Thus a short (few days) storage of the solids results in essentially complete decay of all of the radioisotopes that may be formed and as a result there is no radioactive disposal problem.

The detectors used in this experiment were thallium-activated sodium iodide crystals which were optically coupled to photomultiplier tubes and sealed in aluminum cases (Harshaw type 12S12). These detectors were shielded with lead bricks to strongly attenuate all gamma rays approaching the detectors, except those coming from a selected 1.3-cm-thick cross section of the fluidized bed (see Figure 2). In this arrangement the detectors responded with a signal in proportion to the amount of tracer material in this bed cross section. To eliminate errors due to the horizontal position of the tracer material relative to the detectors, the bed cross section was viewed by two diametrically opposed detector assemblies which placed the detector crystals 30 cm back from the centerline of the bed. By summing the signals from this pair of detectors, a signal was obtained which was essentially independent of the horizontal position of the tracer material. As shown in Figure 1, three such detector pairs were used, one pair near the top of the bed, one pair near the middle of the bed, and one pair viewing a 2.5-cm-high cross section of the shale in the discharge tube. This last detector-pair in effect recorded the rate at which the tracer left the fluidized bed.

The photomultipliers were powered by a single very stable power supply set at about 870 V. Signals from the detectors were first amplified and then screened by a pulse height discriminator which

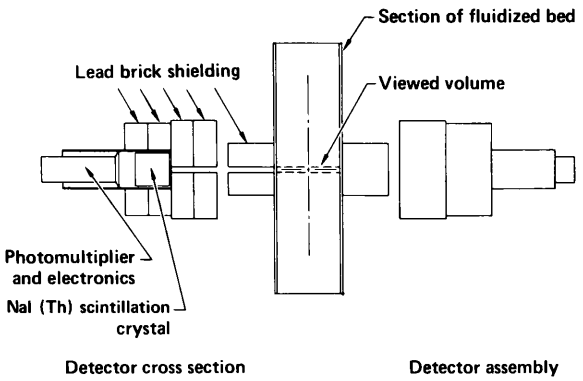

FIGURE 2 - Paired detector and columnator assembly.

passed only those pulses corresponding to 1.78-MeV gamma rays. The pulses from each pair of detectors were then summed and fed to a count rate meter which generated a signal in proportion to the input pulse rate. In addition the rate meter also time-averaged the pulse rate; a 2-s time average was used in this study.

The signals from each of the three rate meters were recorded both on a multichannel strip chart and by a computer-based data acquisition system. This data acquisition system sampled the signal from each rate meter once each second during the experiment. The data were then recorded on tape cassettes. For each experiment the computer also recorded other basic data, such as solids screen size, electronic gain settings, averaging time constants, electronic offset, gas rate, date, and run number.

Because of the nature of the signals obtained, it was important to treat the data very carefully especially with regard to noise and background correction. The data recorded in this study represent a concentration pulse which has a long tail approaching zero with increasing time. Because of the natural decay of the ^{28}Al, the data must be multiplied by a correction factor which increases exponentially with time. If there is no appreciable noise or background count then this is an acceptable situation. However, if the noise plus background is, say, 1% of the peak pulse height and the experiment runs for two half-lives, then because of the decay correction the noise plus background has been multiplied to 4% of peak at a time when the desired signal may be only 1% of peak. In this case the desired signal is completely lost in the noise and background. This problem was ameliorated by the technique described below.

The recorded data were processed through a series of steps to reduce the effects of noise and background on the calculated results of the experiments.

First, the data were numerically averaged by the algorithm

$$y(i) = 0.048[y(i - 3) + y(i + 3)] + 0.093[y(i - 2) + y(i + 2)] + 0.182[y(i - 1) + y(i + 1)] + 0.364y(i)$$

where y(i) is the ith recorded datum and the normalized factors represent an exponential attenuation as one moves each way from the ith datum.

Second, the background was removed from the averaged data by the following sequence: (1) the first 30 data from Channel 3 (at the bed discharge tube) were examined and the arrival time of the first tracer was determined, (2) the average of the Channel 3 data up to (but not including) the arrival of signal was calculated, (3) this average noise and background was subtracted from all data (gain factors were taken into account for Channels 1 and 2), and (4) the data were scanned for the few negative values that appeared after this process, and each of these data were set to zero.

Third, the data were corrected for radioactive decay of the ^{28}Al.

The final step of the data reduction was to integrate the recorded data for Channel 3 and find the times for one-quarter, one-half, and three-quarters of the tracer to be discharged from the bed. This integration was accomplished by the following: (1) the recorded and corrected data were integrated from the beginning to the end of the experiment, and (2) an exponential function was fitted to 30 data from late in the experiment. The data used were either those 30 just following the signal drop to 5% of peak value or, if the experiment ended before 30 additional data were recorded, the last 30 in the experiment. This exponential function was integrated from the time the experiment ended to infinity and the result

added to the integral of the experimental data. Finding the partial discharge times was facilitated by recording the computed integral to each datum as the initial integration was performed. The computer scanned these integral values from the beginning datum forward in time until the selected partial discharge value was exceeded. Then, by interpolation, the time was estimated for that fraction of the tracer to be discharged from the bed.

These times as calculated by the process described above were interpreted as follows: (1) the half integral was assumed to be the median residence time for the tracer sample, and (2) the difference between the three-quarter and one-quarter times was interpreted as the dispersion time of the tracer sample.

The process indicated above was repeated for each of the eight or nine runs made for each selected operating condition. The averages and 90% confidence intervals of the averages of both the median and the dispersion times were calculated.

RESULTS

The results of this study are indicated in Figures 3 through 10 which show the effects of fluidizing gas velocity, particle size, residence time, and particle-size distribution on median time (half integral time) and dispersion time (interquartile time). Figures 3 and 4 show concentration-time histories plotted from the processed data. Figures 5, 6 and 7 illustrate the effects observed when the solids in the bed have a relatively narrow particle-size distribution -0.84, +0.42 mm (-20, +40 mesh)--passing screen size is only twice that of the retaining screen. Figures 8, 9 and 10 show the observations for conditions when the solids in the bed have a relatively broad particle-size distribution -1.68, +0.21 mm (-12, +70 mesh). These figures are discussed in detail below.

Of particular note at this point is the fact that this study offers a new technique for studying the motion of crushed oil shale as it moves through processing equipment. This study clearly demonstrates the usefulness of neutron activation of a short-lived aluminum isotope and a means to detect its presence from outside a process unit.

Figures 3 and 4 show typical concentration-time histories as recorded during two experimental runs. Clearly there is much more information embedded in these records than median and dispersion times. The periodic structure recorded in Figure 4 may reflect a circulation pattern in the bed. The fine structure in these curves may reflect the passage of bubbles or perhaps local bubble interactions.

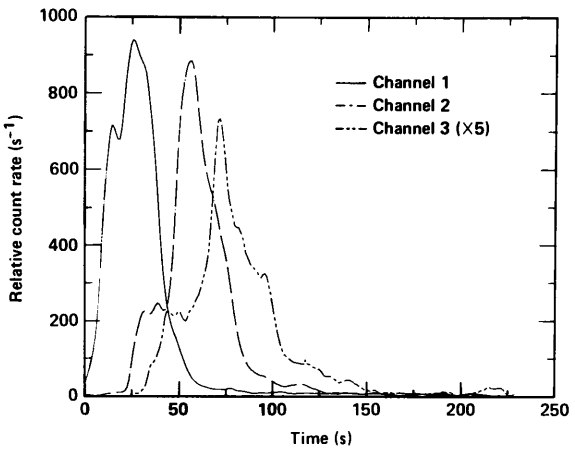

FIGURE 3 - Tracer concentration vs time showing little evidence of circulation.

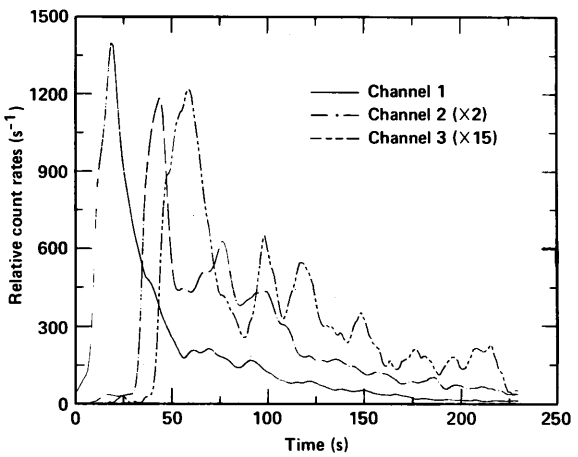

FIGURE 4 - Tracer concentration vs time showing strong evidence of circulation.

Figure 5 illustrates the observed variation of median and dispersion times as a function of nominal residence time (the quantity of solids in

the bed divided by the solids feed rate). For perfect plug flow, median time and nominal residence time would be equal; for a perfectly mixed vessel, the median time would be 69% of nominal residence time. The particle size was -0.84, +0.42 mm (-20, +40 mesh), and the gas rate was 1.2 times the minimum fluidization velocity. Both the median and dispersion times increased with nominal residence time as was expected. However, the median residence time was not proportional to the nominal residence time. The dispersion time was observed to increase almost proportionally with nominal residence time.

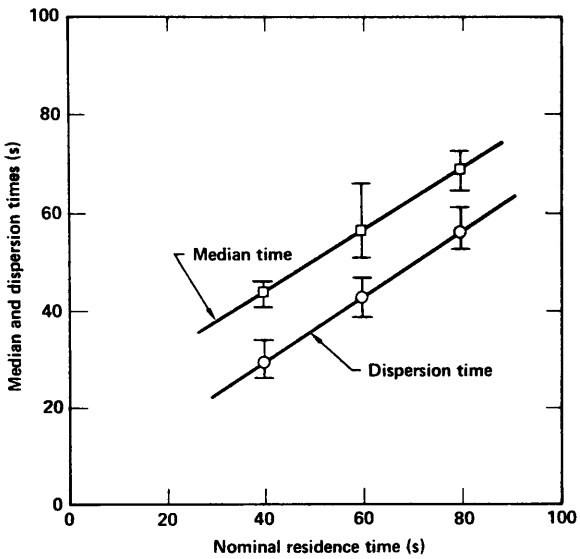

FIGURE 5 - Median and dispersion time vs nominal residence time with a narrow particle-size distribution operating at 1.2 times incipient fluidization velocity.

Figure 6 illustrates the observed variation of median and dispersion times as a function of gas rate. The particle size was -0.84, +0.42 mm (-20, +40 mesh), and the nominal residence time was 60 s. Under these conditions and range of variation, the median residence and dispersion times were observed to decrease slightly with increase in gas velocity. It was observed that the 90% confidence interval of the means for both of these variables diminished by a factor of about five at the higher gas rate indicating more uniform treatment of the solids at higher gas velocities.

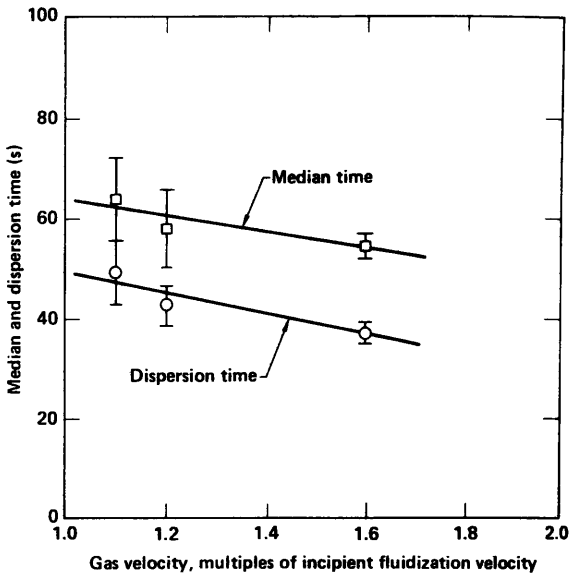

FIGURE 6 - Median and dispersion time vs gas velocity with a narrow particle-size distribution and a 60-s nominal residence time.

Figure 7 illustrates the observed variation of median and dispersion times as a function of solids particle size where the particle-size distribution is narrow. For these data the nominal residence time was 60 s, and the gas velocity was 1.2 times the incipient fluidization velocity. These data show no strong trends in terms of changes in mean results. The significant trend here is that the 90% confidence intervals of the mean are reduced by about an order of magnitude as the particle size is increased from 0.3 to 1.2 mm. This suggests that the process as described here becomes more uniform as particle size increases. However, because the incipient fluidization velocity increases with particle size, the 1.2 times incipient velocity also represents a much greater amount of power input to the bed for larger particles than for small. Because no experiments were run with the small particles with the same gas flow rate as was used for the large particles, it is not clear that particle size is the determining factor.

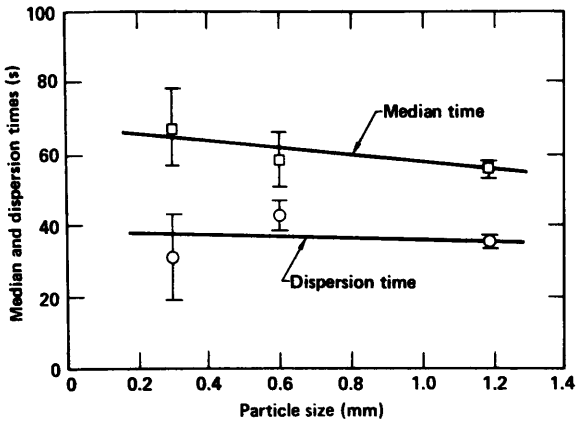

FIGURE 7 - Median and dispersion time vs particle size for 60-s nominal residence time and 1.2 times incipient fluidization velocity.

Figures 8, 9, and 10 illustrate results for experiments where the bed was filled with solids having a broad particle-size range, -1.68, +0.21 mm (-12, +70 mesh). Figure 8 illustrates the variation of median and dispersion times as a function of nominal residence time with a constant gas velocity of 1.2 times the incipient fluidization velocity and a tracer particle size of -0.84, +0.42 mm (-20 +40 mesh). This figure suggests that the median time increases with residence time but perhaps not uniformly. The figure also shows that dispersion time does not uniformly increase with nominal residence time in contrast to the results shown in Figure 5.

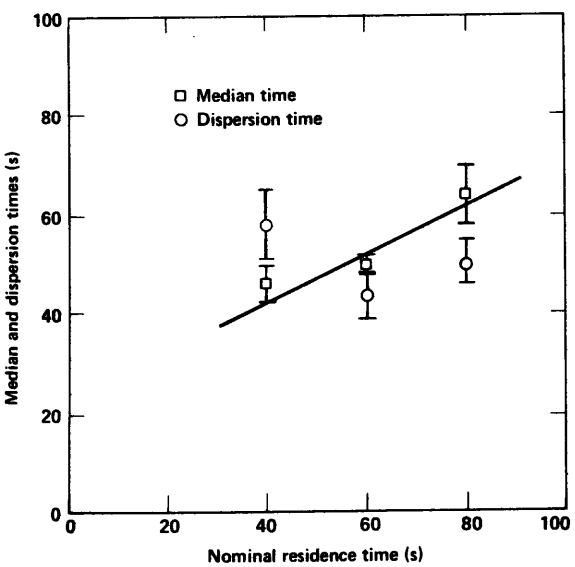

FIGURE 8 - Median and dispersion time vs nominal residence time with broad particle-size distribution and at 1.2 times incipient fluidization velocity.

Figure 9 shows the variations with gas velocity. For this case the median time is not strongly dependent upon gas velocity. The dispersion time shows a definite dependence upon gas velocity. There is a point of concern in that one might expect that the dispersion time should approach zero as the gas velocity approaches incipient fluidization. Note, also, that for higher gas velocities there is an increase in the confidence interval of the mean for dispersion times.

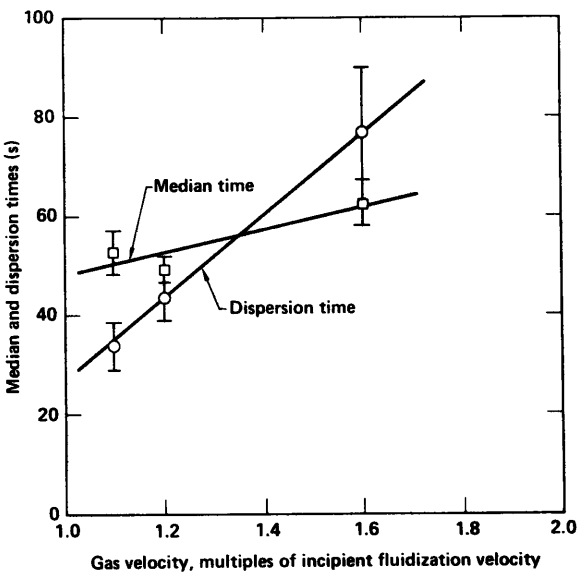

FIGURE 9 - Median and dispersion time vs gas velocity with broad particle-size distribution and a 60-s nominal residence time.

Figure 10 shows the behavior of the three size fractions moving through the bed. For these experiments the tracer material was one of the

three size fractions found in the bed. Thus, the results shown in this figure indicate how each size fraction moves in the bed. This figure shows that as the particles become larger both the median and dispersion times decrease with the greater difference found between the middle and fine size fractions. The results show that the finest cut takes about twice as long as the coarse cut to pass through the bed. The dispersion times also show a factor of about two reduction going from the fine particles to the coarse.

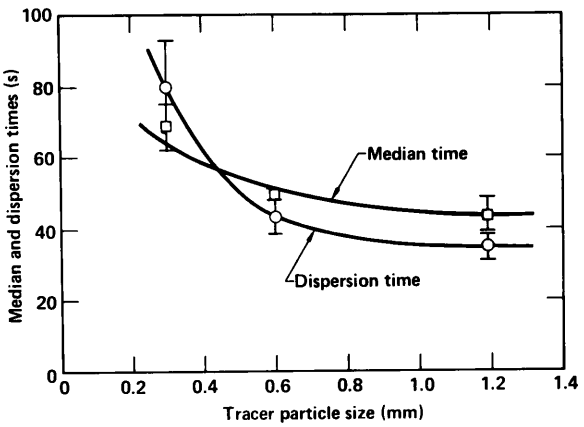

FIGURE 10 - Median and dispersion time vs tracer particle size with broad particle-size distribution in the bed, gas velocity at 1.2 times incipient fluidization velocity, and nominal residence time of 60 s.

CONCLUSIONS

1. The tracking of particles by neutron activation and subsequent gamma ray detection offers a viable means for following oil shale through a process.
2. Computer processing of data as used in this study enhances the value of the data and can lead to a better understanding of the phenomena involved.
3. The behavior of fluidized beds of particles of broad particle-size distribution is significantly different from that of a narrow particle-size distribution. Thus, particular care should be exercised in the design of fluidized beds for commercial use.
4. In a fluidized bed of crushed oil shale having a broad particle-size distribution, the fine particles flow downward more slowly and disperse more than the coarse particles. The path of the fine particles is also more random, showing greater irregularity, than that of the coarse particles.

REFERENCES

1. Christiansen, D. E., Incipient Fluidization Characteristics of Crushed Oil Shale, Lawrence Livermore National Laboratory, Livermore, Calif., report in preparation.
2. Levenspiel, O., and Bischoff, K. B., Advances in Chemical Engineering, Vol. 4, p. 95 (1963).
3. Guide for Experimenters, Rotating Target Neutron Source-II, Lawrence Livermore National Laboratory, Livermore, Calif., Report M-094 Rev. 1, March 1, 1982.

ACKNOWLEDGMENTS

The operating staff of the Rotating Target Neutron Source, under direction of Clinton M. Logan, was very cooperative and helpful in assisting in the neutron irradiation of shale samples.

The mechanical-technical staff under direction of Terrance C. Erven assisted in all phases of this work. Particularly, we thank Calvin W. Hall for careful workmanship in construction of the fluidized bed assembly, and for valuable assistance in initial operation.

Michael J. Muehlbauer provided assistance during much of the equipment operation, and performed preliminary data analysis.

The computer software for data acquisition and storage was prepared by Linda L. Ott.

This work was performed under the auspices of the U.S. Department of Energy by the Lawrence Livermore National Laboratory under contract number W-7405-ENG-48.